Journal of visualization manuscript No.
(will be inserted by the editor)

Visualization and analysis of muzzle flow fields using the Background Oriented Schlieren technique

Abdelhafidh MOUMEN · **Jurgen GROSSEN** ·
Irene NDINDABAHIZI · **Johan GALLANT**

Received: date / Accepted: date

Abstract Several experimental and numerical studies on muzzle blast and flow fields have been performed (Schmidt and Shear (1974), Schmidt and Shear (1975), Schmidt (1984), Klingenberg and M. Heimerl (1992), Fansler (1997)). However, due to the extremely short duration and the spatiotemporal evolution of these flows, experimental quantitative techniques are limited (Klingenberg and M. Heimerl (1992)). As a consequence, the number of validated numerical calculations is limited as well (Schmidt (1984)). On the other hand, although the development of computer models that succeeded in predicting the pressure and velocity measurement, they show at the same time different temperatures and densities (Celmins (1979)). Thus the motivation of this research. The present paper focuses on the development of a density sensitive and non-intrusive measurement technique and the implementation of a quantitative flow visualization method based on Background Oriented Schlieren (BOS) (Meier (2002)) combined with a high-speed camera. In BOS, the experimental set-up of conventional schlieren (mirrors, lenses, and knife-edge) is replaced by a background pattern and a single digital camera (Raffel (2015)). The muzzle flow fields and the flow field around a 5.56 mm projectile in flight were successfully visualized. Indeed, the implemented experimental high-speed BOS set-up has demonstrated its ability to capture clearly the salient features of the precursor and the propellant gas flow fields and their interactions. The captured structures such as vortex, barrel shock, Mach disk, and blast wave show a good agreement with that issued from a realized conventional Schlieren set-up and the bibliography (Schmidt and Shear (1975), Klingenberg and M. Heimerl (1992)). Confirming the BOS capability to visualize complex density flow fields.

Keywords Intermediate ballistics · Flow visualization · Muzzle flow fields · Muzzle blast · Background Oriented Schlieren

Abdelhafidh MOUMEN
Department of Weapon systems and Ballistics, Royal Military Academy, avenue de la Renaissance 30, Brussels, 1000, Belgium
E-mail: abdelhafidh.moumen@gmail.com

1 Introduction

The determination of the muzzle flow filed properties is still a challenge owing to the complexity of the phenomena and the extremely high spatiotemporal evolution. Indeed it occurs within a sphere centered on the muzzle of a radius equal to 100 caliber during less than 10 ms. Thus, a lot of attention has been given to the investigation on intermediate ballistics. First, it aims to understand the dynamics of blast and its interaction with the projectile since it strongly affects its flight control and stability. Second, the deep insight into this process is essential for the development of the muzzle devices aiming at the attenuation of unwanted firearms effects such as the recoil and the sound. Thanks to several experimental studies based upon flow visualization (Erdos and Del Guidice (1975), Schmidt and Shear (1975), Merlen and Dyment (1991)), the muzzle flow field structures are relatively well known. Nevertheless, due to the dusty propellant gas proprieties and the qualitative nature of the aforementioned work, the near-field aerodynamics is not understood as well. Essentially for these reasons, the numerical simulations studies took the challenge. On the other hand, due to the complexity of the phenomena, numerical simulations have to adopt several assumptions. These approximations concern the propellant gas properties, the shock wave propagation model and the friction between the projectile and the barrel. Sweeping the bibliography, we noticed several ambiguities between the most important publications in the domain. This concerns mainly the dynamic shock wave interaction and the projectile/wave interaction. The latter phenomenon is well known by the overtaking process. Thus these studies, aiming at plotting the projectile aerodynamic forces and acceleration, resulted in several differences (Jiang (2003), Watanabe et al. (1995), Rajesh et al. (2007a), Muthukumaran et al. (2012)). In addition, in these studies, although the numerical simulation of the precursor flow matched qualitatively those of the experimental flow visualization, the main propellant flow did not match as well (Cler (2003)). All these cited residual ambiguities impose the need to conduct a systematic study to get more quantitative data from the muzzle flow field.

In the present study, the objective is to visualize quantitatively the muzzle flow filed as it expands into the surrounding atmosphere in order to get a deeper comprehension of these phenomena. Furthermore, we will develop quantitative measurement techniques in order to enhance the body of quantitative experimental data for the comparison with numerical simulations that come in support of other studies dedicated to the development of muzzle devices and the determination of aerodynamic coefficients sets. Various non-intrusive density-sensitive visualization techniques coupled with high-speed camera technology form a potential diagnostic tool in this field. Indeed, the density gradient within the inspected medium affects the light beam original path that it would have followed as for a uniform density. This perturbation may be manifested and thus detected by several ways. The light beam different impingement angles or places are detected by schlieren and shadowgraph techniques which are sensitive to the first and the second derivatives of refraction index respectively (Settles (2001)). On the other hand, the interferometry is sensitive to the density and detects the arrival time delay. Due to its low-cost, simplicity, non-intrusive nature, and unlimited field of view, allowing the visualization of large scale phenomena such as the firing of large-caliber weapons. The BOS is considered as the first potential quantitative flow visualization to investigate the muzzle flow fields at the Accredited Ballistic Applications Laboratory at the Royal Military Academy.

2 Intermediate ballistics

The intermediate ballistics is a branch of ballistics that deals with the phenomena occurring during the transition of the projectile between the interior (in-bore combustion and acceleration of the projectile) and the exterior ballistics (flight dynamics of the projectile). Despite its limited space-time expanse — it occurs in the vicinity of the muzzle during few microseconds — this area of research was always attractive for the ballistician. Indeed, the launch of the projectile and the rapid discharge of a highly hot, compressed and reactive gas is of paramount importance. First, the muzzle flow field development and its interaction with the projectile influences its flight and control behavior (Jiang (2003)). Second, from an operational point of view, reducing the firearms signature such us flash (after-burning process) and sound is important for the reduction of the signature of the troops in the battlefield. Also, from a security stand, the muzzle blast effect and prediction have been extensively studied in order to protect the crew, ammunition, and equipment (Schmidt (1984)). Almost all interventions of the researchers in this part of the ballistics can be subdivided into two parts (Klingenberg and M. Heimerl (1992)). A first part is rather chemical which is based on the modification of the propellant powder via the adjunction of additives. The second is rather mechanical which is based on the study and the development of muzzle devices. In both cases, the successful improvement is only possible after the deep understanding of the muzzle flow field.

In general, the muzzle flow field is characterized by two or three jet flows. Depending upon the weapon interior ballistics and physical dimensions, before the projectile separation from the tube, one or two precursor flow fields are formed in the vicinity of the muzzle. Then after the projectile launch, the combustion gas discharges in the precursor flow field and forms the main propellant flow field.

The main precursor flow features that could be seen in a firearm are depicted in the Fig. 1 which represents the schematic of a precursor flow filed of a small caliber weapon (M-16 rifle) taken from (Klingenberg and M. Heimerl (1992)). It is mainly formed by the air inside the barrel ahead of the projectile and the leakage. The expulsed air exiting from the barrel, derived by the accelerated projectile (piston effect), creates compression waves that coalesce into a normal shock wave. The sudden discharge of this normal shock wave and the compressed air behind it in the ambient air creates a blast wave namely the precursor or the primary blast wave and forms a volume known as the underexpanded jet. Indeed, at the muzzle exiting plan, the compressed air, behind the shock wave, expands forming a Prandtl-Meyer expansion fan. Then, once arrived at the jet boundary, these expansion waves will be reflected to form a series of compression waves that coalesce into a barrel shock. This intercepting shock will be intercepted by a Mach disc across which demarcates the boundary between the supersonic and subsonic velocities. Hence, these two features border the shock-bottle. The size of this supersonic and bonded jet develops and grows with the increase of the muzzle exit pressure ratio P_e/P_0 (with P_e is the exit pressure and P_0 is the ambient pressure). Downstream of the Mach disk, the compressed air which was initially in the barrel and the ambient air that was perturbed earlier by the blast wave form a contact surface.

On the other hand, when the projectile disengages from the muzzle, the combustion gas expands out into the surroundings and interacts with the precursor flow. This main propellant flow field exhibits the same structure as the preceding, namely an underexpanded jet flow encapsulated by a blast wave.

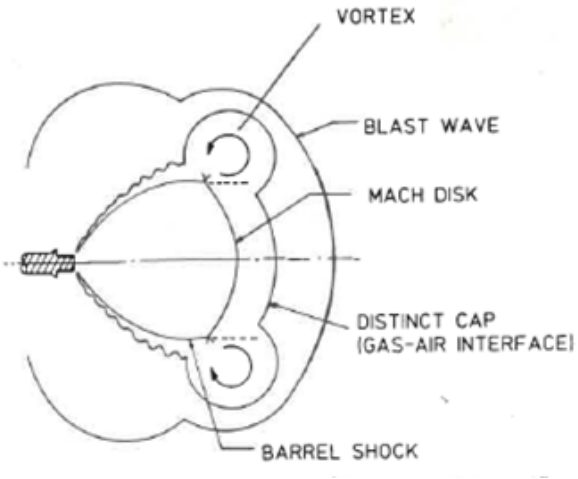

Fig. 1: Schematic of a precursor flow filed of a small caliber weapon (M-16 rifle) (Klingenberg and M. Heimerl (1992))

3 Background Oriented Schlieren Technique (BOS)

3.1 Principles of the BOS

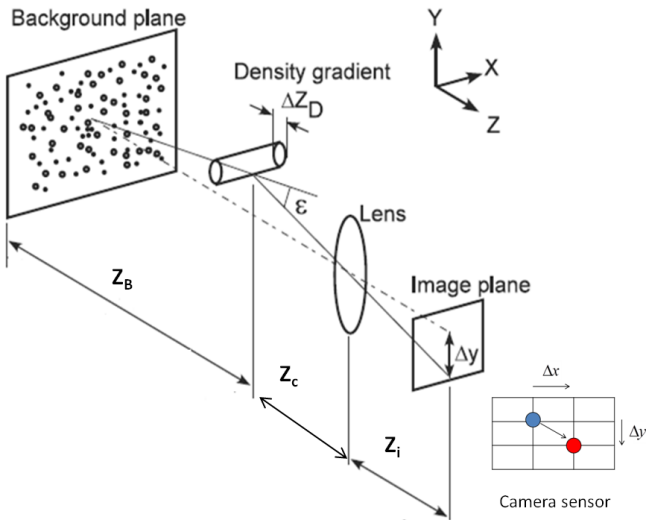

Fig. 2: Simplified optical path in the x-y-z plane in a BOS set up. The dashed line: the path of light with the refractive field. The dotted line: the path of light without refractive index field adapted from (Venkatakrishnan and Meier (2004)).

The Background Oriented Schlieren (BOS) technique originally proposed by Meier (Meier (2002)) is a quantitative measurement tool of refraction index gradients field in transparent media (mainly gas and liquid). The principle of the BOS technique is similar to the conventional Schlieren technique. Indeed, it exploits the deviation of the light passing through a phase object (heterogeneous medium). The classical technique is qualitative in nature and requires several optical equipments such as lenses, mirrors, camera and knife edge. On the other side, BOS employs only an appropriate background and a digital still camera. The set up of the BOS technique consists in a camera that focuses on a background (usually a random dot pattern)— hence the name background oriented— in order to record at least two images of the same background taken with (flow-on) and without (flow-off/tare) the investigated flow. The introduction of the Schlieren object in between the camera and the background produces a deflection of the light rays captured by the camera sensor. Thereby, the resulting image from the second exposure will appear distorted. The second step consists in the calculation of the deflection in the image plane, which can be done by numerical comparison of the two exposures. This evaluation is usually performed by cross-correlation methods obtained from particle imagery velocimetry (PIV) (Settles and Hargather (2017)). The resulting displacements fields are then used to reconstruct the object refraction index field. Indeed, the displacements Δy and Δx measured in the image plane contain information about the refractive index integrated along the line of sight (Fig.2). Assuming a paraxial recording and small deflection ε, the displacement Δy can be expressed as (Raffel (2015)):

$$\Delta y = \frac{f}{Z_B + Z_C - f} \cdot Z_B \cdot \varepsilon_y = M \cdot Z_B \cdot \varepsilon_y \tag{1}$$

with M the magnification factor in the background plane, f the camera lens focal length, Z_B and Z_c are respectively the distances that separate the middle plan of the flow with width Z_D from the background and the camera. The integration of Eikonal equation along the light path yields the relationship between the integrated refraction index and the ε_x and ε_y component of the angular ray deflection ε:

$$\varepsilon_y = \frac{1}{n_0} \cdot \int_{\Delta Z_D} \frac{\partial n}{\partial y} dz \tag{2}$$

Once the displacement fields are determined, the refraction index can be reconstructed by solving the Poisson equation derived from Equations 1 and 2 (Beermann et al. (2017)):

$$\frac{\partial^2 n}{\partial^2 x} + \frac{\partial^2 n}{\partial^2 y} = -\frac{2n_0}{\Delta Z_D \cdot (\Delta Z_D + 2Z_B)} \cdot \left(\frac{\partial \Delta y}{\partial y} + \frac{\partial \Delta x}{\partial x}\right) \tag{3}$$

with n_0 the reference refractive index. Thanks to the Gladstone-Dale law, the density can be directly retrieved:

$$n - 1 = k\rho \tag{4}$$

where n denotes the refractive index, ρ stands for the density of the medium, and k denotes the Gladstone-Dale coefficient which depends on the fluid composition and the wavelength used.

3.2 Setup geometry

The determination of the experimental set-up dimensions is essentially based on the calculation of the sensitivity and the spatial resolution in order to visualize a given flow. The optimization of these two important criteria is mandatory to obtain reliable quantitative and qualitative information. Once the acceptable resolution and sensitivity are fixed the emplacement of the different BOS set-up component can be determined.
The sensitivity S is defined as the ratio between the minimum detectable displacement Δy to the correspondent angle of ray deflection ε (Gojani et al. (2013)):

$$S = \frac{\Delta y}{\varepsilon} \tag{5}$$

Since $\Delta y = M \cdot Z_B \cdot \varepsilon$, the sensitivity may be expressed as :

$$S = M.Z_B = \frac{f}{Z_B + Z_C - f} Z_B \tag{6}$$

A necessary condition for the displacement to be detected with an acceptable signal to noise ratio is that the pattern shift Δy must be larger than the camera sensor pixel size (Goldhahn and Seume (2007)). To overcome this limitation, we aim to increase the ray deflection in the image plane. Based on this equation, one can assess that the sensitivity is a function of the camera characteristics and the set-up dimensions. To enhance the BOS system sensitivity, we should first increase the focal length f and choose a camera with a small sensor pixel size (pix). Second, the background to the flow distance must be as large as possible. This latter guiding is limited by the fact that the camera sensor needs to capture at least a point with known refraction index (boundary condition for the Poisson equation), the blurring effect (Raffel (2015)), and the system spatial resolution.
From an optical point of view, the BOS system resolution can be defined as the highest spatial frequency that is still possible to be detected (Goldhahn and Seume (2007)). Similar to the sensitivity, the spatial resolution is also a function of the camera characteristics (f, $f\#$ (the lens f-number), pix) and the set-up geometry. Based on the development in (Gojani et al. (2013)), a good approximation of the spatial resolution is expressed by :

$$A = \frac{Z_B}{Z_B + Z_C} . \frac{f}{f\#} \tag{7}$$

Note that the spatial resolution is approximated by the sensitivity divided by the lens aperture $f\#$. Hence, the enhancement of the sensitivity leads to a decrease of the resolution which means that a trade-off of the location of the investigated object in between the camera and the background must be found. Indeed, a flow nearer to the background reduces the blurring effect, since the camera is in sharp focus on the background, and gives place to a better capture of shock waves (Nicolas et al. (2017)) at the risk of filtering of the low-density gradients. Although, the spatial resolution can be attenuated by increasing the f-number what itself is limited by the available light intensity and the blurring effect.

3.3 BOS backgrounds

In order to detect the wide range of the density gradients common in the muzzle flow fields, special attention was given to the used background. The background construction is function

of several parameters such as the density gradients, the camera characteristics, and the post-processing tool. The advantage of BOS in comparison with PIV is the full control of the background pattern. Indeed, problems like in-plan loss and peak locking are avoided due to the control of the particles density, shape and size. As mentioned before, a background pattern has to permit the evaluation of the displacement field usually named optical flow in the vision computer community. In order to fulfill this mission, it must exhibit a high spatial frequency with a large inhomogeneity (Raffel (2015)). The most popular BOS Background is the random dot pattern. This background is originally the transposition of the PIV image in a paper. As the technique developed, since 2000, several other types of backgrounds were proposed: the colored background (CBOS), the colored grid background (CGBOS) and the wavelet noise (this is in addition of the natural background already used by Loose et al. (2000). Leopold (2007) was the first, in 2007, to propose the CBOS. Thereby, in addition to the black (or white) dots, he used the primary colors to generate the colored background. He assumed that the correlation based on three colored channels (plus the black one) offers more precision and spatial resolution as for every measurement eight independent correlations instead of one can be performed. Ota et al. (2010) proposed a striped colored pattern called the CGBOS. The advantage of this technique in comparison to the CBOS is that it does not require a reference image under the flow-off condition. The wavelet noise pattern is proposed by Cook and DeRose (2005) and first used by Atcheson et al. (2009). Opposed to the random dot patterns which are optimal for only a one distance meaning that the background has to be changed with any change in set up geometry, the wavelet noise feature is considered as a multi-scale and a multi-resolution pattern. More recently Meier and Roesgen (2013) employed the pattern speckle of a laser as a background.

Based on rules from both the PIV community (Scarano and Riethmuller (1999)) and the parametric study by Vinnichenko et al. (2012), the design of a fully optimized pattern is reduced to the determination of the particle size and their density. In summary, these rules may be cited as follows;

- In general, the random dot pattern performs better than the regular and the wavelet noise.
- Although its practicality and ease of use, the wavelet noise pattern does not respond well to blur produced by the phase object.
- The random dot pattern with a dot size of 25 pixels is recommended, though 23 pixels gives better sensitivity (Raffel (2015)).
- The interrogation window size has to be greater than four times the estimated displacement.
- The number of particles N per interrogation window (also called density or population) must be greater than 10.

3.4 Experimental setup

Following the different guidelines cited previously, the pattern was generated and was printed on a transparent film. A Photron FASTCAM SA-X2 camera equipped with 1-Megapixel CMOS image sensor (20.48 x 20.48 mm, 1024 x 1024 pixels, 20-micron pixel size) and a Nikon lens 50-300 mm f/2.7-22, shooting at 3 μs exposure was used. A f-number equal to 16 was selected to limit the effect of the light diffraction (Nicolas et al. (2017)). The investigated object was the muzzle flow of a 5.56 mm weapon with a projectile muzzle velocity $V_0 = 950m/s \pm 10$ (Fig. 3).
The most important challenge in the present case is to carry out an experimental set-up

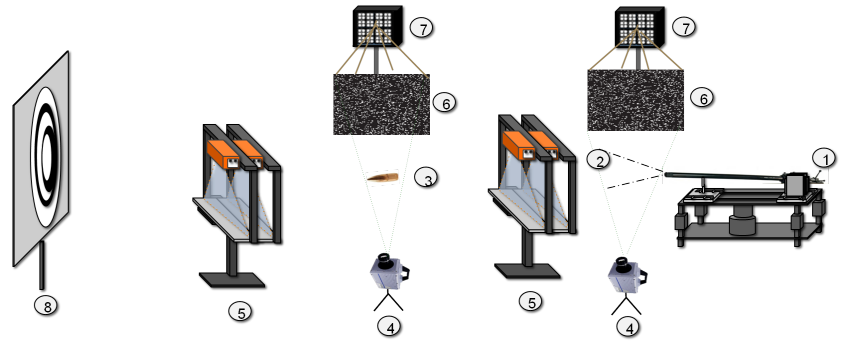

Fig. 3: Schematic representation of the built BOS set-up
1: weapon system 2: muzzle flow filed 3: projectile in flight 4: high speed camera 5: velocity light gates 6: background 7: backlight 8: target

that is able to capture the different dynamic phenomena, occurring within a very short time (400 μs). Indeed, it is a question of visualizing the development and the shrinking of a jet going from a very highly underexpanded (shock bottle structure) to a moderately underexpanded jet (diamond structure) plus the propagation of blast waves, all being formed by molecules of air and/or propellant gas. This is to make a compromise between the high sensitivity allowing the capture of the details of the underexpanded jet and the spatial resolution allowing the clear visualization of the blast waves development at the cost of lower sensitivity. To do this, a set of tests with different geometrical dimensions and camera parameters was realized (see table. 1). The post-processing tool used during this study was PIVLab (Thielicke and Stamhuis (2014)). For the PIV algorithm, a 50% multi-grid linear fast transform window deformation algorithm with subsequent window sizes of 64, 32 and 16 is chosen. The sub-pixel interpolation was realized by a 2x3 point Gaussian interpolation method.

Table 1: Experimental set-up

Test	Z_B (mm)	Z_C (mm)	f (mm)	$f\#$	Frame rate$/s$
1	665	2190	105	16	30,000
2	665	2190	105	16	40,000
3	665	2190	80	16	40,000
4	1000	2620	200	16	30,000

4 Results and Discussion

4.1 Validation of the results

To examine the ability of the BOS technique to accurately capture the muzzle flow fields, several similar cases were chosen for a qualitative comparison. First, the captured features of the precursor flow field were compared, (Fig. 4(a)), with the schematic development of the

M-16 rifle precursor flow and, an antecedent frame was compared with a realized shadowgraph of a precursor flow (Fig. 4(b)). It can be seen from the comparison that the agreement between the BOS result and the available data is very good. Indeed, the locations and the shape of the precursor blast wave, the Mach disk, the contact discontinuities are matching very well with the schematic development, the shadowgraphy and schlieren images. It is also seen that the barrel shock and the vortex ring structures are well captured by the BOS.

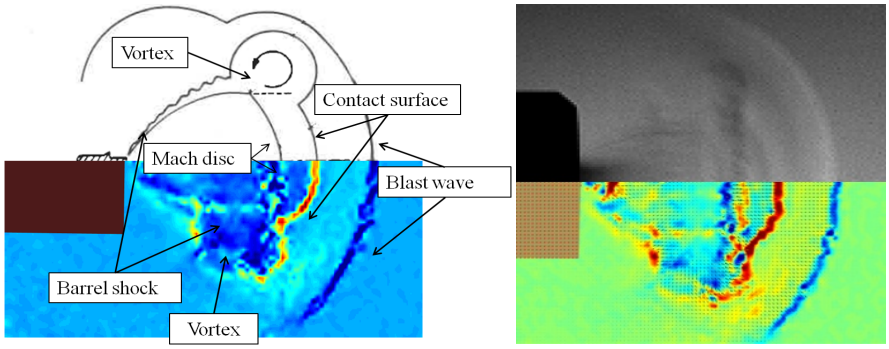

4(a) 4(b)

Fig. 4: Comparison between BOS results (lower half) and (a) (upper half) schematic of the precursor flow and (b) (upper half) a realized shadowgraph

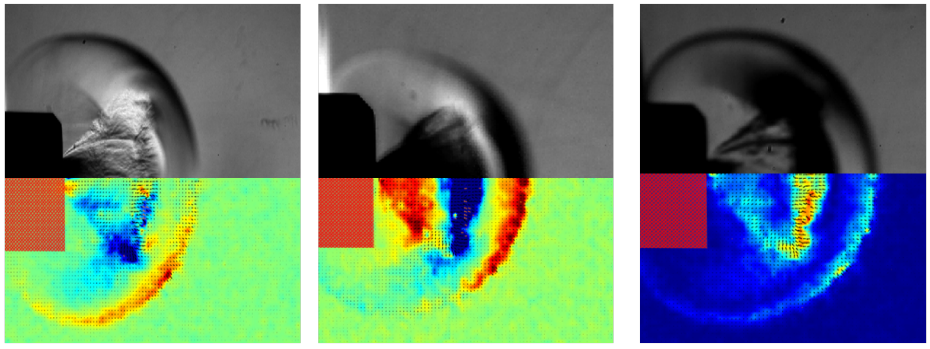

Fig. 5: Comparison between BOS results (lower half) and realized schlieren images with different knife edge orientation: (left) vertical displacements vs horizontal knife edge - (center) vertical displacements vs vertical knife edge - (right) magnitude of the displacements vs circular knife edge

Furthermore, due to the lack of an oriented knife edge in comparison with the conventional schlieren, the BOS technique is able to capture simultaneously the gradients $\partial\rho/dx$ and $\partial\rho/dy$ in the horizontal and vertical directions, respectively. In order to verify simultaneously this aforementioned quality and the qualitative accuracy of the BOS, three tests were conducted with different knife edge orientations with similar conditions as in the BOS. In

Fig. 5 the BOS vertical, horizontal and the magnitude of the displacements are compared respectively with schlieren images with horizontal, vertical and circular knife edges. The confrontation of the position and the shape of the compared features shows a good harmony between the two techniques. The small differences in brightness noticed in this comparison are due to the difference in sensitivity between the two techniques, which is a function of the overall set-up geometry and the camera characteristics for the BOS and mainly the knife edge position for the classical schlieren.

Fig. 6 shows a comparison of propellant flow field development capture from the two techniques. The locations and the shape of the projectile, blast wave, the bow shock, and the barrel shock match very well.

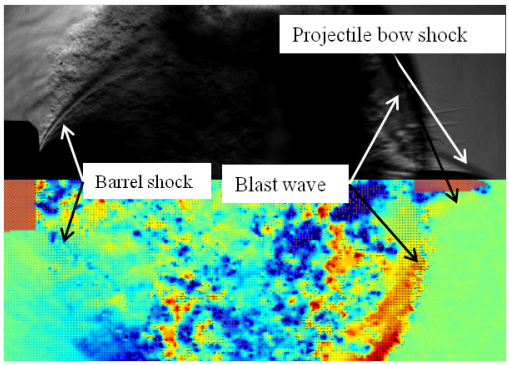

Fig. 6: Vertical displacements at $t = 0.133\ \mu s$

4.2 Precursor flow field visualization

In comparison with the main propellant flow, the precursor flow, which mainly air, has the advantage to be clearly visible through the various density sensitive visualization techniques. This makes it easier to discern the different captured muzzle flow features. In order to distinguish the different structure borders, the BOS results will be presented by the vertical displacement relative to $\partial\rho/dy$, the gradients of the displacements, and/or the magnitude of the displacements are relative to $\partial\rho/dx$ and $\partial\rho/dy$. The projectile disengagement from the barrel is considered as the time scale origin and all the image axes are in mm. The vectors point in the direction of lower density and the colors show their magnitude in pixel per frame with red being the highest.

At $t = -225\ \mu s$ the primary phenomena of the precursor flow development are captured. It consists only of a simple sphere shape formed at the immediate exit of the barrel by the expulsed air.

At $t = -200\ \mu s$, the precursor flow field pattern appears (Fig. 7). Indeed the underexpanded jet form encapsulated by a spherical blast wave is visible. The precursor blast wave (1) is located at x = 50 mm. Since it propagates into the atmosphere, the blast wave develops a nearly spherical form with a center downstream of the muzzle. The Mach disk (3) is observed at x = 38 mm, it forms with the two barrel shock (4) the shock bottle shape which demarcates the boundary of the supersonic/subsonic flow regions. The contact surface (2) separating gas initially outside the tube from that which was inside is seen downstream from

the latter structure. It has a mainly spherical shape but it is constrained by the presence of the primary vortex ring (5). The bi-colored cone (6) at the immediate exit of the muzzle (7) represents the Prandtl-Meyer expansion fan which separates the high pressure upstream (in-bore) from the expanded gas downstream.

Another capture of the precursor flow at $t = -66\ \mu s$ is shown in the Fig. 8. At this phase,

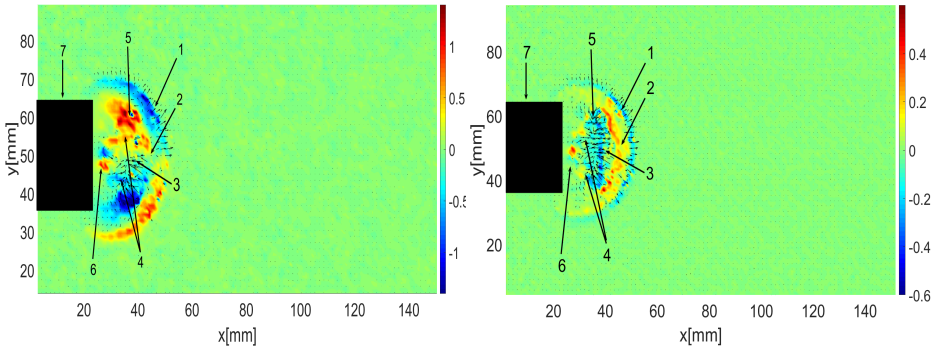

7(a) Vertical displacements relative

7(b) Gradient of the displacements

Fig. 7: Precursor flow at $t = -200\ \mu s$,
1: the precursor blast wave 2: the contact surface 3: the Mach disk 4: the barrel shock 5: the vortex ring - 6: the Prandtl-Meyer expansion fan 7: the muzzle

the nearly spherical expanding blast wave (1) propagates further downstream in the ambient air and its strength diminishes. Also, the unrestrained underexpanded jet develops and its salient features are clearly distinguished. Indeed, the shock bottle bounded by the barrel shock (4) and the Mach disk (3) is seen formed without disturbing. This shock bottle is situated between the jet boundary (8) and the vortex rings (5) in the lateral direction and the contact surface in the axial downstream direction. Due to its greater sensitivity, the best capture of the very highly underexpanded jet was realized by the set-up number 4 (Table 1) at the same moment $t = -66\ \mu s$ (Fig. 9).

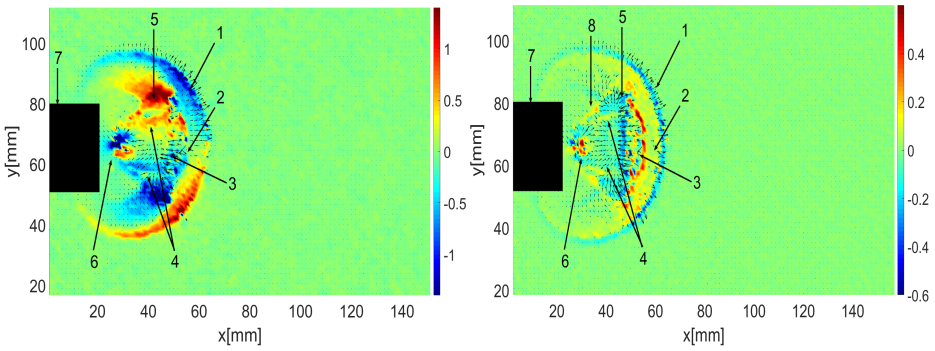

8(a) Vertical displacements

8(b) Gradient of the displacements

Fig. 8: Precursor flow at $t = -66\ \mu s$, 1-7: see legend figure 7.

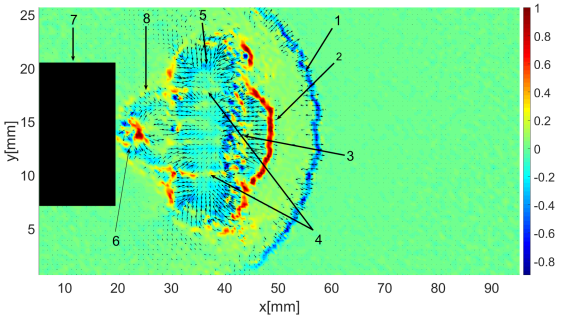

Fig. 9: Gradient of the displacements of the precursor flow at$t = -66\ \mu s$, 1-7: see legend figure 7 8: the jet boundary.

The latter phase of the precursor flow before the bullet ejection is shown in Fig. 10 taken at $t = -33\ \mu s$. This part of the development is characterized by two new phenomena. We observe first, the appearance of the front portion of the projectile (9) which will be immersed in an underexpanded environment, a fact that has its impact on the projectile dynamic drag coefficient (Gopalapillai et al. (2007)). Second, the presence of a small amount of gas propellant leakage. At this time, the underexpanded core is slightly disturbed at its origin but the Mach disk (3) and the contact surface (4) are still undisturbed. The outer blast wave (1) continues its propagation spherically upstream and downstream.

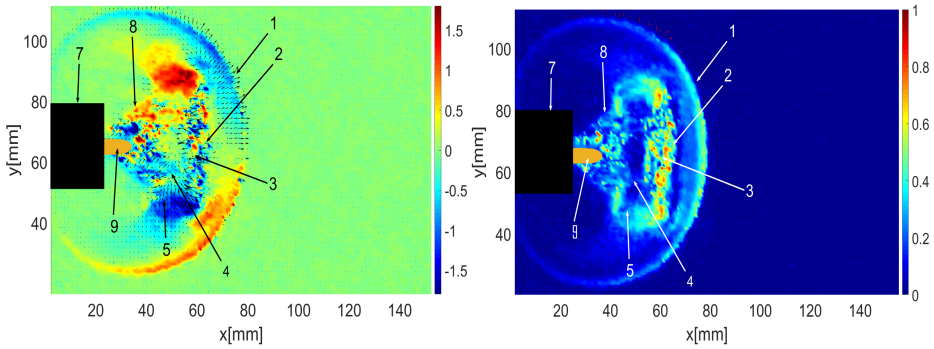

10(a) Vertical displacements

10(b) Magnitude of the displacements

Fig. 10: Precursor flow at $t = -33\ \mu s$, 1-8: see legend figure 9 9: the projectile

4.3 Main propellant flow field visualization

The expansion of the high pressure gas produced from the combustion of the propellant powder into the surroundings constitutes the second main process. This occurs in the same way as the first flow after the uncorking of the barrel with the exception that this second flow develops in an ambient region with lower pressure and density. In this phase, neither the flow field development nor wave interaction is clearly observable due to the dusty propellant gas.

Right after the projectile complete separation from the barrel, at $t = 66\ \mu s$, Fig 11, the main propellant gas (3) discharges in the vicinity of the muzzle (5) and the main blast wave (4) starts to exit the gun barrel. The strong interaction of the main propellant flow with the preceding is clearly visible through the ellipsoid form of the main blast wave. This blast wave propagates mainly in the radial direction and partly in the rear direction where it is clearly visible. This anisotropic form is created due to the interaction with the precursor flow and the directed nature of the emptying process. Indeed, if we fire in a vacuum and without leakage, thus without precursor flow, then the muzzle blast wave would be less distorted (Merlen and Dyment (1991)). By analogy with shock waves generated by an explosion this "peer like-shape" blast wave could be retrieved in the case of a directed energy release, this is typically the case of a cylindrical explosive with a detonator attached along to its axis (Mizukaki et al. (2015)). It is also seen that the leading edge of this second blast wave is unapparent. This disappearance may be explained by the fact that this region is characterized by a low density and pressure due to the flow overexpansion making the blast overpressure invisible (Jiang (2003)). Furthermore, the forward development of the underexpanded jet core and the second blast wave is constrained by the presence of the projectile (2). Indeed, the underexpanded jet form of the main flow is formed and restrained by the projectile base but is not visualized. This form will appear later once the turbulence and the dust have decreased. Regarding the projectile, no bow shock is observed at its front so we may conclude that it moves subsonically in respect to the local flow condition (Watanabe et al. (1995)). Although the precursor supersonic underexpanded jet is already overtaken, the primary shock wave continues to propagate spherically without any disturbance.

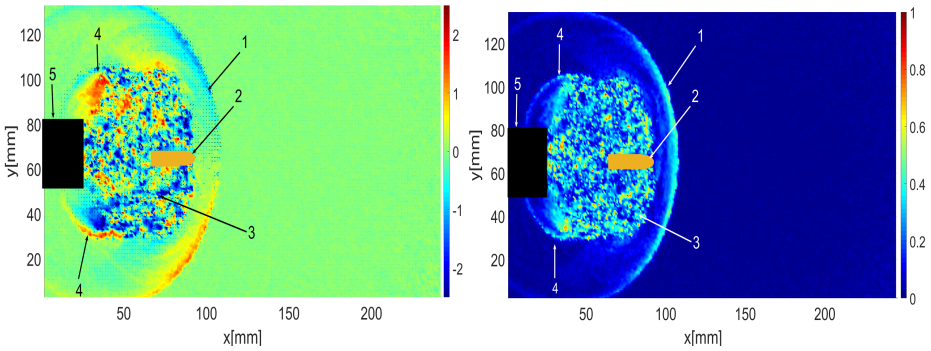

11(a) Vertical displacements

11(b) Magnitude of the displacements

Fig. 11: Main propellant flow development at 66 μs,
1: the precursor blast wave 2: the projectile 3: the propellant gas 4: the main blast wave 5: the muzzle

As the projectile (2) continues to move downstream, at $t = 100\ \mu s$ (Fig 12.), the leading edge of the second blast (4) reappears at its shoulder. The front portion of the projectile has just traveled through the precursor shock wave. These two projectile/shock wave interactions lead to a complex flow phenomenon that may hardly affect the flight control and stability of the projectile (Rajesh et al. (2007b)). The two blast waves conserve their original shape namely spherical and elongated for the precursor and the main blast respectively.

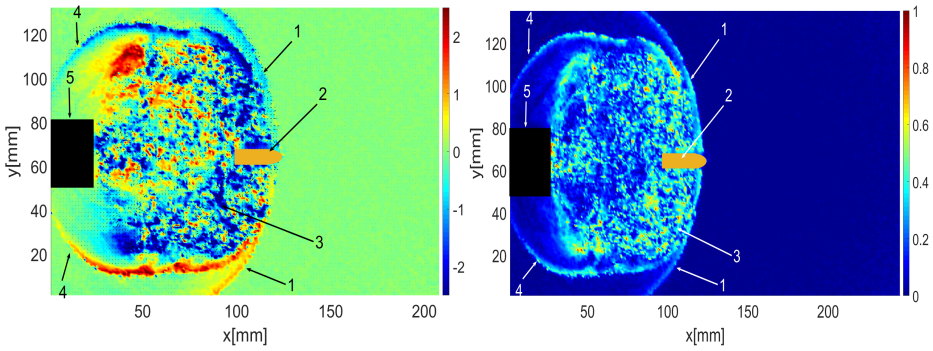

12(a) Vertical displacements

12(b) Magnitude of the displacements

Fig. 12: Main propellant flow development at 100 μs, 1-5: see legend figure 11.

Figure 13 shows the main propellant flow situation at $t = 133\ \mu s$. Almost two-thirds of the projectile (2) has overtaken the preceding shock waves (1) and (4). The projectile Mach number increases suddenly and only at this moment, the bow shock (6) is established at its tip as it enters the quiescent air. Also, at this moment, the second blast wave has overtaken the first blast wave. The subsequent frame taken at $t = 166\ \mu s$ shown (Fig. 14), shows that the projectile has totally overtaken the shock wave and is now on a free flight. Indeed, the shock wave, the compression and expansion waves and the wake behind it are clearly captured. The main blast wave continues its propagation downstream and tends to reach the spherical shape as it moves away from the muzzle.

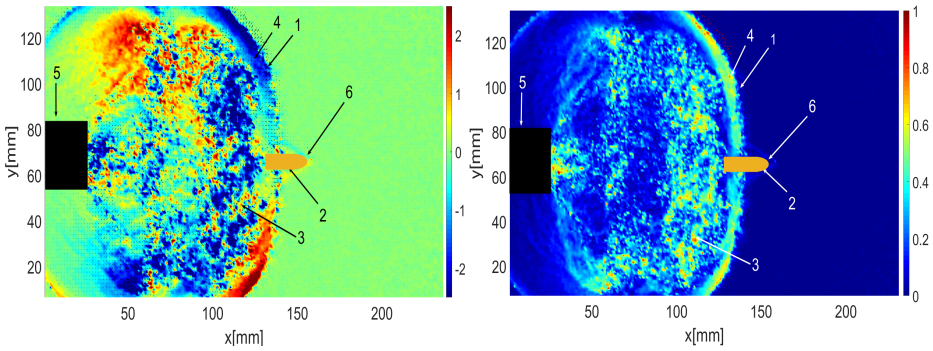

13(a) Vertical displacements

13(b) Magnitude of the displacements

Fig. 13: Main propellant flow development at 133 μs. $1-5$: see legend figure 11 6: the bow shock.

At this phase, the projectile and the blast wave propagate far enough from the muzzle which permits the underexpanded form to take place freely and to be visible. The lateral shocks of the shock bottle (7) are already visible since the time $t = 166\ \mu s$ at the Fig. 14. Then at time $t = 300\ \mu s$ (Fig. 15), once the turbulent gas ball propagates forward we noticed

the first clear appearance of the supersonic core behind it, bounded by both the Mach disk (8) and the barrel shocks (7) in the axial and the lateral direction respectively, also the main blast wave (4) is still visible in the camera field of view.

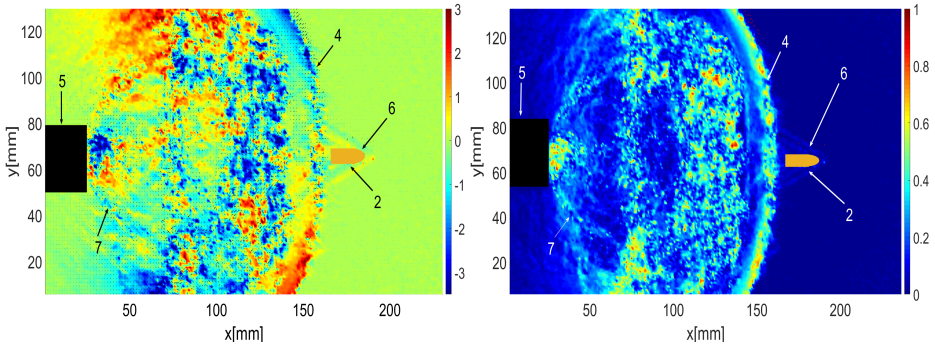

14(a) (Vertical displacements

14(b) Magnitude of the displacements

Fig. 14: Main propellant flow development at 166 μs, $1-6$: see legend figure 13.

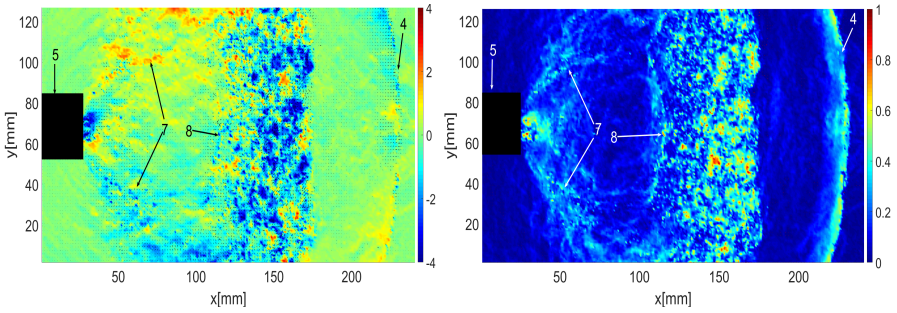

15(a) Vertical displacements

15(b) Magnitude of the displacements

Fig. 15: Main propellant flow development at 300 μs
$1-6$: see legend figure 13 7: the barrel shock 8 the Mach disk

As the gas exist pressure ratio P_e/P_0 continue to increase, the extremely underexpanded form continues to grow up and more specifically the Mach disk continues to move downstream. This occurs until $t = 350$ μs when it becomes quasi-stationary for approximately 40 μs at the locus $x/d = 17.08$. This behavior is in perfect agreement with what is mentioned in the bibliography (Schmidt and Shear (1974)).
As the existing pressure starts to decrease at t=390 μs, the normal inner shock retracts up to the muzzle and the overall shock bottle structure shrinks (Fig 15.a and b taken respectively at $t = 1.056$ ms and $t = 2.41$ ms). This decay follows the pattern of a steady underexpanded jet obeying the empirical law for the Mach disc location (Schmidt and Shear (1974)) :

$$\frac{x}{d} = 0.70 \cdot \sqrt{\frac{\gamma_e . P_e}{P_0}} \tag{8}$$

with γ_e the propellant gas specific heat ratio. As the pressure ratio continues to decrease we reach the following stages :

- First a highly underexpanded jet characterized by a principal core bounded by a Mach disk followed by successively reflected shocks. This usually takes place for an exit pressure ratio 2 to 4 (Franquet et al. (2015)) (figure 16(c) at $t = 5\ ms$)
- Then, a moderately underexpanded jet, characterized by the absence of the Mach dick thus the reflection occurs successively in the symmetry axis to form a series of shock waves also known as the diamond pattern. This usually takes place for an exit pressure ratio of $1,1$ to 3 (Franquet et al. (2015)) (figure 16(d)) at $t = 5.54\ ms$)

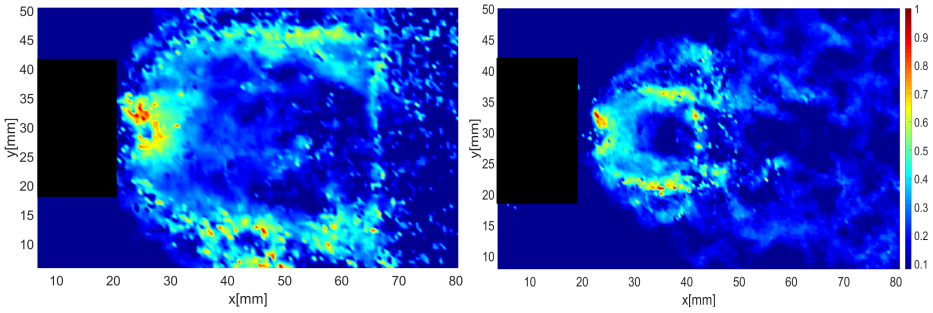

16(a) $t = 1.056\ ms$

16(b) $t = 2.41\ ms$

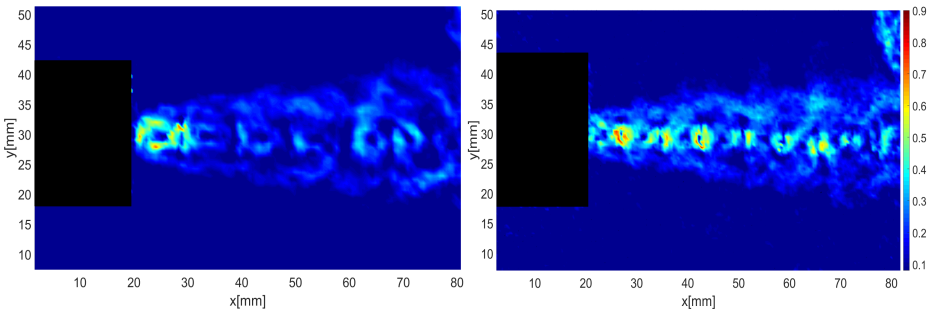

16(c) $t = 5\ ms$

16(d) $t = 5.54\ ms$

Fig. 16: Quasi-steady emptying process : magnitude of displacement which is proportional to $d\rho/dx$ and $d\rho/dy$

5 Conclusion and perspectives

The muzzle flow field of a 5.56 mm gun was visualized based on the relatively novel technique the Background Oriented Schlieren. The two distinct but interacting flow fields namely the precursor and propellant gas were successfully observed by this non-intrusive and quantitative technique. The salient features of the muzzle flow fields were well captured and the results ware validated by comparison with realized schlieren and shadowgraphy images. The interactions between the different flows, blast waves, and the projectile were

discussed. The results presented here confirm the ability of the cited technique to analyze the muzzle flow filed qualitatively and quantitatively. Furthermore, its simplicity and unlimited field of view may make it a convenient tool for the visualization in the field of ballistic especially when large scale flows must be visualized such as large caliber muzzle flow field and projectile in flight. During the tests, once the gun barrel warms up, we noticed the appearance of a second precursor flow, besides the first one described previously. This is due to a propellant gas leakage. This phenomenon will be discussed in a future publication together with the quantitative (density based) analysis of the muzzle flow fields and in-bore velocity and pressure measurements.

Acknowledgements The authors would like to acknowledge the team of the Accredited Ballistic Applications Laboratory at the Royal Military Academy.

References

Atcheson B, Heidrich W, Ihrke I (2009) An evaluation of optical flow algorithms for background oriented schlieren imaging. Experiments in Fluids 46(3):467–476, DOI 10.1007/s00348-008-0572-7

Beermann R, Quentin L, Pösch A, Reithmeier E, Kästner M (2017) Background oriented schlieren measurement of the refractive index field of air induced by a hot, cylindrical measurement object. Applied Optics 56(14):4168, DOI 10.1364/AO.56.004168

Celmins A (1979) Theoretical accuaracy of acoustic gas temperature measurements in guns. Tech. Rep. ARBRL-TR-02134, USA Ballistic Research Laboratory, ABERDEEN PROVING GROUND, MARYLAND

Cler D (2003) CFD Application to Gun Muzzle Blast - A Validation Case Study. In: 41st Aerospace Sciences Meeting and Exhibit, American Institute of Aeronautics and Astronautics, Reno, Nevada, DOI 10.2514/6.2003-1142

Cook RL, DeRose T (2005) Wavelet Noise. CM Trans Graphics (Proc SIGGRAPH) 24, 3 (July), 803–811

Erdos J, Del Guidice PD (1975) Calculation of Muzzle Blast Flowfields. AIAA Journal 13(8):1048–1055, DOI 10.2514/3.60503

Fansler KS (1997) Description of Gun Muzzle Blast by Modified Ideal Scaling Models:. Tech. rep., Defense Technical Information Center, Fort Belvoir, VA, DOI 10.21236/ADA330051

Franquet E, Perrier V, Gibout S, Bruel P (2015) Free underexpanded jets in a quiescent medium: A review. Progress in Aerospace Sciences 77:25–53, DOI 10.1016/j.paerosci.2015.06.006

Gojani AB, Kamishi B, Obayashi S (2013) Measurement sensitivity and resolution for background oriented schlieren during image recording. Journal of Visualization 16(3):201–207, DOI 10.1007/s12650-013-0170-5

Goldhahn E, Seume J (2007) The background oriented schlieren technique: Sensitivity, accuracy, resolution and application to a three-dimensional density field. Experiments in Fluids 43(2-3):241–249, DOI 10.1007/s00348-007-0331-1

Gopalapillai R, Kim HD, Setoguchi T, Matsuo S (2007) On the near-field aerodynamics of a projectile launched from a ballistic range. Journal of Mechanical Science and Technology 21(7):1129–1138, DOI 10.1007/BF03027663

Jiang Z (2003) Wave dynamic processes induced by a supersonic projectile discharging from a shock tube. Physics of Fluids 15(6):1665, DOI 10.1063/1.1566752

Klingenberg G, M Heimerl J (1992) Gun Muzzle Blast and Flash, Progress in Astronautics and Aeronautics, vol 139. Washington, DC : American Institute of Aeronautics and Astronautics

Leopold F (2007) The Application of the Colored Background Oriented Schlieren Technique (CBOS) to Free-Flight and In-Flight Measurements. In: 2007 22nd International Congress on Instrumentation in Aerospace Simulation Facilities, IEEE, Pacific Grove, CA, USA, pp 1–10, DOI 10.1109/ICIASF.2007.4380894

Loose S, Richard H, Dewhirst T, Raffel M (2000) Background oriented schlieren (BOS) and particle image velocimetry (PIV) applied for transonic turbine blade investigations. In: 10th International Symposium on Applications of Laser Techniques to Fluid, p 8

Meier AH, Roesgen T (2013) Improved background oriented schlieren imaging using laser speckle illumination. Experiments in Fluids 54(6):1549, DOI 10.1007/s00348-013-1549-8

Meier G (2002) Computerized background-oriented schlieren. Experiments in Fluids 33(1):181–187, DOI 10.1007/s00348-002-0450-7

Merlen A, Dyment A (1991) Similarity and asymptotic analysis for gun-firing aerodynamics. Journal of Fluid Mechanics 225(-1):497, DOI 10.1017/S0022112091002148

Mizukaki T, Borg S, Danehy PM, Murman SM, Matsumura T, Wakabayashi K, Nakayama Y (2015) Background-Oriented Schlieren for Large-Scale and High- Speed Aerodynamic Phenomena. In: 53rd AIAA Aerospace Sciences Meeting53rd AIAA Aerospace Sciences Meeting, Kissimmee, Florida, p 10, DOI https://doi.org/10.2514/6.2015-1692

Muthukumaran CK, Rajesh G, Kim HD (2012) The Launch Dynamics of Supersonic Projectiles. Journal of Spacecraft and Rockets 50(6):27, DOI https://doi.org/10.2514/1.A32466

Nicolas F, Donjat D, Léon O, Le Besnerais G, Champagnat F, Micheli F (2017) 3D reconstruction of a compressible flow by synchronized multi-camera BOS. Experiments in Fluids 58(5):46, DOI 10.1007/s00348-017-2325-y

Ota M, Hamada K, Maeno K (2010) Quantitative 3D density measurement of supersonic flow by Colored Grid Background Oriented Schlieren (CGBOS) TECHNIQUE. In: 27th International Congress of the Aeronautical Sciences, p 7

Raffel M (2015) Background-oriented schlieren (BOS) techniques. Experiments in Fluids 56(3):60, DOI 10.1007/s00348-015-1927-5

Rajesh G, Kim HD, Matsuo S, Setoguchi T (2007a) A study of unsteady projectile aerodynamics using a moving coordinate method. Proceedings of the Institution of Mechanical Engineers, Part G: Journal of Aerospace Engineering 221(5):691–706, DOI 10.1243/09544100JAERO227

Rajesh G, Kim HD, Matsuo S, Setoguchi T (2007b) A study of unsteady projectile aerodynamics using a moving coordinate method. Proceedings of the Institution of Mechanical Engineers, Part G: Journal of Aerospace Engineering 221(5):691–706, DOI 10.1243/09544100JAERO227

Scarano F, Riethmuller ML (1999) Iterative multigrid approach in PIV image processing with discrete window offset. Experiments in Fluids 26(6):513–523, DOI 10.1007/s003480050318

Schmidt EM (1984) Muzzle Blast Pressure Loadings upon Aircraft Surfaces:. Tech. rep., Defense Technical Information Center, Fort Belvoir, VA, DOI 10.21236/ADA139132

Schmidt EM, Shear D (1975) Optical Measurements of Muzzle Blast. AIAA Journal 13(8):1086–1091, DOI 10.2514/3.60506

Schmidt EM, Shear DD (1974) The flow field about the muzzlepf an H-16 rifle. Tech. Rep. AD916646, USA Ballistic Research Laboratory, Aberdeen proving gound , Maryland

Settles G (2001) Schlieren and Shadowgraph Techniques: Visualizing Phenomena in Transparent Media. Engineering Online Library, Springer Berlin Heidelberg

Settles GS, Hargather MJ (2017) A review of recent developments in schlieren and shadowgraph techniques. Measurement Science and Technology 28(4):042001, DOI 10.1088/1361-6501/aa5748

Thielicke W, Stamhuis E (2014) PIVlab – Towards User-friendly, Affordable and Accurate Digital Particle Image Velocimetry in MATLAB. Journal of Open Research Software 2(1):e30 DOI http://dx.doi.org/10.5334/jors.bl

Venkatakrishnan L, Meier GEA (2004) Density measurements using the Background Oriented Schlieren technique. Experiments in Fluids 37:11, DOI DOI 10.1007/s00348-004-0807-1

Vinnichenko NA, Uvarov AV, Plaksina YY (2012) Accuracy of Backgroudn Oriented Schlieren for fifferent background patterns and means of refraction index reconstruction. In: 15th International Symposium on Flow Visualization, Minsk, Belarus, p 15

Watanabe R, Fujii K, Higashino F (1995) Numerical simulation of the flow around a projectile passing through a shock wave. In: 13th Applied Aerodynamics Conference, American Institute of Aeronautics and Astronautics, San Diego,CA,U.S.A., DOI 10.2514/6.1995-1790